Atmos. Meas. Tech., 10, 825–837, 2017
www.atmos-meas-tech.net/10/825/2017/
doi:10.5194/amt-10-825-2017

Atmospheric Measurement Techniques
Open Access
EGU

Simultaneous retrieval of water vapour, temperature and cirrus clouds properties from measurements of far infrared spectral radiance over the Antarctic Plateau

Gianluca Di Natale, Luca Palchetti, Giovanni Bianchini, and Massimo Del Guasta

Istituto Nazionale di Ottica – CNR, Sesto Fiorentino, Italy

Correspondence to: Luca Palchetti (luca.palchetti@ino.it)

Received: 25 May 2016 – Discussion started: 12 August 2016
Revised: 20 January 2017 – Accepted: 4 February 2017 – Published: 8 March 2017

Abstract. The possibility separating the contributions of the atmospheric state and ice clouds by using spectral infrared measurements is a fundamental step to quantifying the cloud effect in climate models. A simultaneous retrieval of cloud and atmospheric parameters from infrared wideband spectra will allow the disentanglement of the spectral interference between these variables. In this paper, we describe the development of a code for the simultaneous retrieval of atmospheric state and ice cloud parameters, and its application to the analysis of the spectral measurements acquired by the Radiation Explorer in the Far Infrared – Prototype for Applications and Development (REFIR-PAD) spectroradiometer, which has been in operation at Concordia Station on the Antarctic Plateau since 2012. The code performs the retrieval with a computational time that is comparable with the instrument acquisition time. Water vapour and temperature profiles and the cloud optical and microphysical properties, such as the generalised effective diameter and the ice water path, are retrieved by exploiting the 230–980 cm^{-1} spectral band. To simulate atmospheric radiative transfer, the Line-By-Line Radiative Transfer Model (LBLRTM) has been integrated with a specifically developed subroutine based on the δ-Eddington two-stream approximation, whereas the single-scattering properties of cirrus clouds have been derived from a database for hexagonal column habits. In order to detect ice clouds, a backscattering and depolarisation lidar, co-located with REFIR-PAD has been used, allowing us to infer the position and the cloud thickness to be used in the retrieval. A climatology of the vertical profiles of water vapour and temperature has been performed by using the daily radiosounding available at the station at 12:00 UTC. The climatology has been used to build an a priori profile correlation to constrain the fitting procedure. An optimal estimation method with the Levenberg–Marquardt approach has been used to perform the retrieval. In most cases, the retrieved humidity and temperature profiles show a good agreement with the radiosoundings, demonstrating that the simultaneous retrieval of the atmospheric state is not biased by the presence of cirrus clouds. Finally, the retrieved cloud parameters allow us to study the relationships between cloud temperature and optical depth and between effective particle diameter and ice water content. These relationships are similar to the statistical correlations measured on the Antarctic coast at Dumont d'Urville and in the Arctic region.

1 Introduction

Cirrus clouds have a strong effect on the Earth radiation budget (Cox et al., 2010; Harries et al., 2008; Kiehl and Trenberth, 1997; Liou, 1986; Lubin et al., 1998) and on the determination of the overall climate sensitivity (Baran et al., 2014; Hardiman et al., 2015; Cox et al., 2015). However, their radiative impact is still uncertain (Maestri et al., 2005; Baran, 2007; Stoker et al., 2013) since they show a very strong variability in coverage extent and altitude (Mahesh et al., 2005) as well as in the crystal size/shape distribution (Sassen et al., 2008; Baum et al., 2005a, b; De Leon and Haigh, 2007). As reported by Baran (2009), the Earth–atmosphere radiation balance depends upon many different parameters characterising cirrus clouds, such as geometrical thickness, particle size and shape distribution (PSD) of ice crystals and most of all the optical depth. Furthermore their coverage is still not

well characterised and spans from about 30 % of the planet surface at any given time to 70 % in tropical areas (Wylie and Menzel, 1999), so their climate effect could be very important.

The strongest radiative effect of cirrus occurs in the atmospheric window region (8–12 µm) and is highly dependent on the cloud optical thickness. The contribution of the far infrared region (FIR) below 667 cm^{-1} (wavelength > 15 µm) is also very important (Maestri et al., 2014) because in this region the emitted spectrum is extremely sensitive to the cloud particle effective diameter, in particular for small particle sizes ($\simeq$ 20–30 µm). The sensitivity to the effective diameter is enhanced in the FIR because of the strong modulation of the imaginary part of the refractive index of ice (Lynch et al., 2002; Baran, 2007), which has a peak at 800 cm^{-1} and a minimum at 400 cm^{-1}.

The FIR region is also very important since it represents up to 45 % percent of the entire thermal flux emitted by the Earth (Harries et al., 2008), thus the flux modulation induced by clouds has an important effect on the energy balance. However, in the FIR the effect of cloud overlaps with the water vapour rotational absorption band; hence it is difficult to disentangle the two competing effects (Maestri and Holtz, 2009). Wideband spectral measurements are essential for trying to separate the atmospheric state and cloud components of the climate system (Huang et al., 2010).

The determination of cloud infrared spectral properties is even more important in polar regions since, due to lower temperatures, more of the radiation exchange happens in the FIR region, and cloud contribution to the modulation of the outgoing emission, which drives the polar climate, is stronger (Barton et al., 2014; Choi et al., 2010; Lubin et al., 2015; Pithan et al., 2014; Scott and Lubin, 2015). Unfortunately, the lack of measurements caused by the challenging environmental conditions, especially in Antarctica, have prevented the achievement of a reliable characterisation of the cloud radiative impact (Bromwich et al., 2012). The retrieval of cloud microphysical properties from infrared spectral measurements is therefore of great interest because it would allow us to directly relate the cloud microphysics to radiative properties (Cox et al., 2014; Turner, 2005; Mahesh et al., 2001a, b).

In this paper we describe a retrieval process that uses the atmospheric emission in the spectral region between 230–980 cm^{-1} to simultaneously discriminate and evaluate both the thermal contributions of water vapour and cirrus clouds. The process is then used for the analysis of the spectrally resolved measurements of the atmospheric radiance performed over the Antarctic Plateau in very dry conditions. The Radiation Explorer in the Far InfraRed – Prototype for Applications and Development (REFIR-PAD) spectroradiometer (Palchetti et al., 2005; Bianchini et al., 2006) is very suitable for this purpose since it is one of the few operative instruments able to detect the whole infrared atmospheric radiance between 100–1400 cm^{-1} (7–100 µm), covering the entire pure rotational band of water vapour in the FIR (Palchetti et al., 2008; Bianchini et al., 2008). The instrument is installed at Dome C, at the Italian–French station of Concordia, on the Antarctic Plateau (75°06′ S, 123°20′ E) at 3233 m a.s.l., and it has been acquiring atmospheric-emitted radiance spectra almost continuously since December 2011, both in clear- and cloudy-sky conditions. Simultaneous measurements performed by a backscattering and depolarisation lidar (Del Guasta et al., 1993), daily radiosoundings and data from a weather station located on the roof of the physics shelter, where REFIR-PAD is installed, have been also used in the retrieval procedure.

Since the REFIR-PAD field campaign in Antarctica has been going on for more than 4 years, a very large database of spectral measurements (Palchetti et al., 2015) has been collected. The development of a retrieval algorithm able to analyse the entire database will allow us to perform reliable statistics about the radiative contribution of the Antarctic atmosphere and ice clouds.

The modelling of clouds is a hard problem to solve since the exact distributions of crystals size and habits are highly variable, which means clouds are very inhomogeneous in space and in internal structure as well as in time. The assumption of a single uniform layer is typically used to describe the radiative effect of ice cirrus clouds since these clouds are optically thin (Mahesh et al., 2001b) and the internal stratification shows a small effect on the radiative transfer; see also e.g. Turner et al. (2003) and Turner (2005) where the same approximation is used. Furthermore, this assumption has been verified in our specific cases, where the optical depth of cirrus clouds is generally less than 1.2, finding that the effect of considering the stratification produces a difference that is negligible with respect to the measurement noise.

Currently there is very little information about the statistical distribution of shapes of ice particles in polar regions, e.g. Mahesh et al. (2001b) for Antarctica and Turner et al. (2003) for the Arctic show the predominance of column particles. In particular, Turner et al. (2003) showed that the typical polar habits are essentially composed of hexagonal columns with a minor fraction of droxtal for small particles. Furthermore, the available single-scattering models are very few (Fu and Liou, 1993; Fu et al., 1998; Yang et al., 2005) and not validated over the whole spectral range because of the lack of measurements in the FIR. The model developed by Fu et al. (1998) has been chosen in this analysis because it effectively describes clouds composed of a mixture of hexagonal columns where the shape approximates the droxtal for small-sized particles with an aspect ratio near to 1.

The algorithm described in this work makes other assumptions to simplify and optimise the simulations. The δ-Eddington two-stream approximation has been applied to simulate the radiative transfer through the cloud layer, as considered appropriate for single layer clouds (Turner, 2005). The downwelling and upwelling radiances incident at the cloud top and bottom respectively, as well as the down-

ward radiance propagating from the cloud to the observer, are simulated by the Line-By-Line Radiative Transfer Model (LBLRTM) (Clough et al., 2005). The retrieval code is an optimal estimation based on the Levenberg–Marquardt approach (Marquardt, 1963) in which the retrieved parameters are effective particle diameter and ice water path (IWP) for the cloud and some selected points of the vertical profiles of water vapour and temperature. The a priori information is given by the seasonal climatology compiled using the 12:00 UTC daily radiosoundings, and also takes into account the statistical correlations between water vapour and temperature.

The modelling of the atmosphere in the presence of ice clouds by using the single-scattering properties derived from the database compiled by Fu et al. (1998) for an ice crystal mixture of hexagonal columns is described in detail in Sect. 2. The procedure to retrieve the cloud properties and the atmospheric variables is delineated in Sect. 3, starting from the generation of the a priori climatological profiles and the variance-covariance matrix (VCM). The procedure to choose the atmospheric levels to be retrieved is also explained in Sect. 4. Finally, in Sect. 5, the retrieval performance is discussed.

2 Modelling of the thermal radiance emitted by cirrus clouds

The modelling of the infrared spectral radiance emitted by the atmosphere in the presence of cirrus clouds has been performed with the same approach used to fit cloud parameters during Testa Grigia field campaigns in 2007 and 2011 (Palchetti et al., 2016).

The δ-Eddington two-stream approximation of the radiative transfer equation (RTE) for a thermally inhomogeneous scattering layer in case of zenith-looking configuration has been used, as suggested by Deeter and Evans (1998):

$$I_E(0) = e^{-\tau} I(\tau) + \frac{D_b}{1-\beta}\left(1 - e^{\tau(\beta-1)}\right) + \frac{D_+}{1-\lambda}\left(1 - e^{\tau(\lambda-1)}\right) + \frac{D_-}{1+\lambda}\left(1 - e^{-\tau(\lambda+1)}\right), \quad (1)$$

where $I_E(0)$ and $I(\tau)$ are the radiances at the cloud top and bottom respectively. The coefficients D_-, D_+ and λ are reported in Appendix A of Deeter and Evans (1998) and depend on the upwelling and downwelling radiances and the single-scattering properties of the ice particles, i.e. the single-scattering albedo ω, the asymmetry factor g and the optical depth τ. The β coefficient is given, according to Fu (1991) and Fu and Liou (1993), by

$$\beta = \frac{1}{\tau} \ln \frac{B_1}{B_0}, \quad (2)$$

where B_0 and B_1 are the Planck functions calculated at the temperatures of the cloud top and bottom respectively.

Different works were performed to parameterise the single-scattering properties for the large variety of ice crystal habits as a function of the cloud microphysics (Yang et al., 2001, 2005; Wiser and Yang, 1998). In this work we assume a homogeneous distribution of crystal shapes of the hexagonal column type and the approximation of a single uniform layer for the cloud vertical structure.

The single-scattering coefficients that depend on the microphysical properties (D_{ge}, IWP) are given by Fu et al. (1998):

$$\begin{aligned} \tau &= \mathrm{IWP}\left(a_0 + \frac{a_1}{D_{\mathrm{ge}}} + \frac{a_2}{D_{\mathrm{ge}}^2}\right), \\ \tau_{\mathrm{a}} &= \frac{\mathrm{IWP}}{D_{\mathrm{ge}}}\left(b_0 + b_1 D_{\mathrm{ge}} + b_2 D_{\mathrm{ge}}^2 + b_3 D_{\mathrm{ge}}^3\right), \\ g &= c_0 + c_1 D_{\mathrm{ge}} + c_2 D_{\mathrm{ge}}^2 + c_3 D_{\mathrm{ge}}^3, \end{aligned} \quad (3)$$

where D_{ge} is the generalised effective diameter defined as Fu (1996):

$$D_{\mathrm{ge}} = \frac{\int_{L_{\min}}^{L_{\max}} L D^2 n(L) \mathrm{d}L}{\int_{L_{\min}}^{L_{\max}} \left(DL + \frac{\sqrt{3}}{4} D^2\right) n(L) \mathrm{d}L}. \quad (4)$$

D, L and $n(L)$ in Eq. (4) are the width, the maximum dimension and the size distribution of the ice crystals respectively. The coefficients a_i, b_j and c_k in Eq. (3) are tabulated between 3–100 µm in (Fu et al., 1998), and τ_{a} denotes the absorption optical depth. The single-scattering albedo is obtained from the following relation:

$$\omega = 1 - \tau_{\mathrm{a}}/\tau. \quad (5)$$

The optical parameters are scaled to take into account the strong forward peak of the scattering according to Joseph and Wiscombe (1976) as

$$\begin{aligned} \tau' &= \left(1 - \omega g^2\right)\tau \\ g' &= \frac{g}{(1+g)} \\ \omega' &= \left(1 - g^2\right)\frac{\omega}{\left(1 - \omega g^2\right)}. \end{aligned} \quad (6)$$

The wave number dependence of these parameters is shown in Fig. 1 for different values of D_{ge}. As expected, due to the wavelength dependence of the imaginary part of the refractive index of ice (Lynch et al., 2002), the particle scattering is more sensitive to the variation of the effective diameter in the FIR spectral range than in the atmospheric window between 800–980 cm^{-1} (see also Baran, 2007 and Palchetti et al., 2016). On the contrary, the maximum of extinction occurs around 700–800 cm^{-1}, mainly due to the effect of ice absorption.

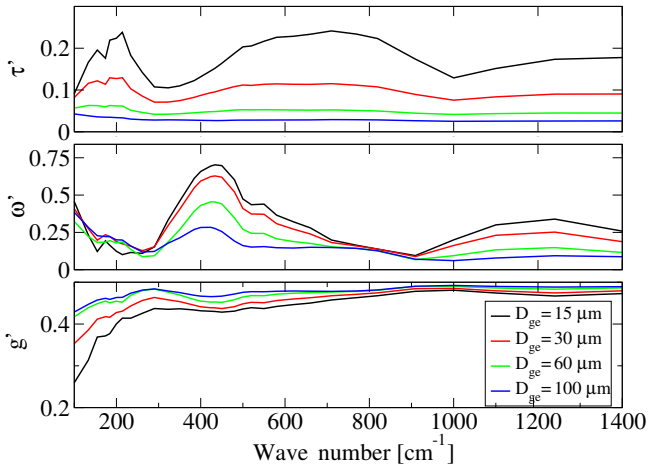

Figure 1. Scaled optical parameters for different values of D_{ge}. The optical depth τ is calculated for IWP $= 2\,g\,m^{-2}$.

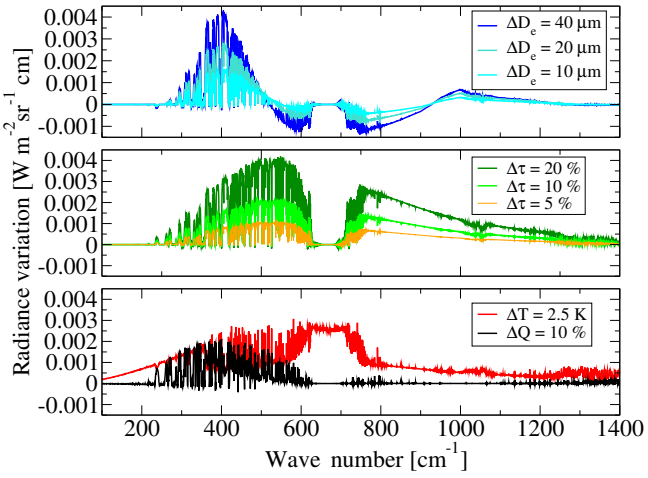

Figure 2. Radiance sensitivity to parameter variation for a summer atmospheric state and a cirrus cloud of 1 km with the bottom at 1800 m above ground, $\tau = 1$ and $D_e = 40\,\mu m$.

Following Baran (2007) and Rathke and Fisher (2000), the final parameters to be used in the radiative transfer model described in the following sections, are further scaled to take into account the gas contribution in the cloud layer yielding the following:

$$\begin{aligned} \tau_t &= \tau + \tau_g \\ \omega'' &= \omega' \frac{\tau'}{\tau'_t} \\ g'' &= g' \frac{\tau'}{\tau'_t}, \end{aligned} \tag{7}$$

where τ_g represents the optical depth of the gases calculated using LBLRTM.

A sensitivity study has been performed to compare the different responses of radiance to atmospheric state and cirrus cloud parameter variations. We have considered a typical case simulated using climatological water vapour and temperature profiles (see Sect. 4 for more details about the used climatological profiles) and a cirrus cloud of 1 km with the bottom at 1800 m above ground and $\tau = 1$. Figure 2 shows that a variation of 10 % in the water vapour volume mixing ratio (Q) has the same effect as a 10 µm variation in D_e in the FIR, but above 500 cm^{-1} the behaviour is the opposite. Therefore the effects of these two parameters can be discriminated in spectral measurements including both spectral regions. Moreover Fig. 2 also shows that the effect of a variation in the cloud τ and D_e can be discriminated by using the FIR spectral range. Finally we note that the temperature variation mainly affects the CO_2 spectral band, with the smaller effect outside this band due to the indirect temperature variation that is assigned to the cloud.

3 Retrieval algorithm

The simulation of the downwelling spectral radiance at the instrument level is performed by dividing the atmosphere into 52 levels with irregular vertical resolution. The vertical resolution varies from 2 m in the first layer above the instrument, where the values and variations of the main atmospheric variables are very large, up to 1 km in the upper part of the profile, around 11 km and close to the tropopause, where the atmosphere is almost transparent. The cloud temperature is calculated from the atmospheric profile as the average between the values at the top and the bottom of the cloud, which are supplied by the lidar measurements.

The retrieved variables are D_{ge} and the IWP for the cloud and the volume mixing ratio (VMR) of water vapour (Q) and the temperature (T) at selected levels of the vertical profiles as described later in Sect. 4. The remaining levels of the vertical profiles are interpolated. The molecular species, for which the VMR is not fitted, are supplied by climatological profiles after Remedios et al. (2007). The initial guesses for the water vapour and temperature profiles, as well as the a priori information, are obtained by the seasonal climatology as described in Sect. 4. The retrieval is limited to the spectral region between 230–980 cm^{-1} where the sensitivity to the selected fitting variables is maximum (see Fig. 2).

The retrieval requires the inversion of the following equation:

$$\boldsymbol{y} = \mathbf{F}(\boldsymbol{x}) + \boldsymbol{\epsilon}, \tag{8}$$

where $\mathbf{F}$ is the forward model, $\boldsymbol{y}$ and $\boldsymbol{\epsilon}$ are the vectors of the measurement and its uncertainty respectively, and $\boldsymbol{x} = (D_{ge}, \mathrm{IWP}, Q, T)$ is the state vector of the system composed by the cloud and the atmospheric contribution for the selected levels of the vertical profiles.

An optimal estimation approach is used for the retrieval of $\boldsymbol{x}$ by means of the minimisation of the cost function:

$$\chi^2 = (\boldsymbol{y} - \mathbf{F}(\boldsymbol{x}))^T \mathbf{S}_\epsilon^{-1} (\boldsymbol{y} - \mathbf{F}(\boldsymbol{x})) + (\boldsymbol{x} - \boldsymbol{x}_\mathrm{a})^T \mathbf{S}_\mathrm{a}^{-1} (\boldsymbol{x} - \boldsymbol{x}_\mathrm{a}), \quad (9)$$

where $\boldsymbol{x}_\mathrm{a}$ is the vector of the a priori information that we assumed coincident with the initial guess, and $\mathbf{S}_\epsilon$ and $\mathbf{S}_\mathrm{a}$ represent the measurement and the a priori VCMs respectively.

The measurement VCM is calculated as follows (Ceccherini and Ridolfi, 2010):

$$(\mathbf{S}_\epsilon)_{ij} = \langle \boldsymbol{\epsilon}\boldsymbol{\epsilon}^T \rangle = \boldsymbol{\delta}_{ij} \left(\mathrm{NESR}_j^2 + (\sigma_\mathrm{F})_j^2 \right) + \varepsilon_i \cdot \varepsilon_j, \quad (10)$$

where the symbol $\langle\ \rangle$ denotes the expectation value, $\boldsymbol{\delta}_{ij}$ is the identity matrix, NESR is the noise equivalent spectral radiance, and $\boldsymbol{\epsilon}$ is the calibration error of the measurement (Bianchini and Palchetti, 2008). σ_F is the forward model error due to the uncertainties in the non-fitted species and the assumption in the description of the cloud properties. The term with the NESR and σ_F denotes the uncorrelated statistical error, whereas the term of products $\epsilon_i \cdot \epsilon_j$ represents the correlated error component given by the calibration uncertainty with a correlation equal to 1, as derived from Planck's law of emission. The forward model error σ_F is dominated by the uncertainty on the CO_2 climatological profile, which is obtained by means of the standard deviation σ_{CO_2} of the CO_2 profile (Remedios et al., 2007) and the derivative of the forward model with respect to the CO_2 volume mixing ratio. The other non-fitted atmospheric species, the single layer approximation and the choice of hexagonal columns for the cloud description have a negligible effect on the VCM compared to the measurement noise.

On the other hand, the a priori VCM has been obtained as a block matrix:

$$\mathbf{S}_\mathrm{a} = \begin{pmatrix} \mathbf{S}_\mathrm{cld} & \mathbf{0} \\ \mathbf{0} & \mathbf{S}_\mathrm{atm} \end{pmatrix}, \quad (11)$$

where $\mathbf{S}_\mathrm{cld}$ is the diagonal VCM for cloud parameters expressed as

$$\mathbf{S}_\mathrm{cld} = \begin{pmatrix} \sigma_{D_\mathrm{ge}}^2 & 0 \\ 0 & \sigma_\mathrm{IWP}^2 \end{pmatrix}, \quad (12)$$

The $\mathbf{S}_\mathrm{atm}$ matrix is the VCM of the atmospheric profiles in which the off-diagonal elements are not null and take into account the correlations between each fitted atmospheric level and also between temperature and water vapour profiles.

Since only a few measurements of cirrus cloud parameters in the Antarctic plateau are available to perform a rigorous statistical analysis of the correlation between D_e and IWP and between these parameters and the atmospheric state, we have chosen not to constrain the retrieval with these a priori correlations. Therefore the off-diagonal elements of $\mathbf{S}_\mathrm{a}$ and $\mathbf{S}_\mathrm{cld}$ are set to be equal to 0. In this way, the results of the simultaneous fitting of the cloud parameters and the atmospheric state will highlight the existing correlation between these variables.

The standard deviations of D_ge and IWP in the 2×2 diagonal matrix of Eq. (12) have been set to be large enough not to be serious constraints (Turner, 2005). If $\boldsymbol{x} = (Q, T)$ represents the vector of the atmospheric radiosounding of water vapour (Q) and temperature (T) then $\mathbf{S}_\mathrm{atm}$ can be calculated from the expectation value:

$$(\mathbf{S}_\mathrm{atm})_{ij} = \frac{1}{N-1} \sum_{k=1}^{N} \left[(x_{ik} - \overline{x}_i) \left(x_{jk} - \overline{x}_j \right) \right], \quad (13)$$

where i, j are the forward model level indexes and k represents the radiosounding index. The $\overline{x}$ denotes the average profile obtained from N radiosoundings. We note that the terms of Eq. (13) with the same index $i = j$ correspond to the measured variance values.

The following iterative formula (Marquardt, 1963) has been implemented by using a Levenberg–Marquardt approach:

$$\boldsymbol{x}_{i+1} = \boldsymbol{x}_i + \left(\mathbf{K}_i^T \mathbf{S}_\epsilon^{-1} \mathbf{K}_i + \gamma \mathbf{D}_i + \mathbf{S}_\mathrm{a}^{-1} \right)^{-1} \left[\mathbf{K}_i^T \mathbf{S}_\epsilon^{-1} (\boldsymbol{y} - \mathbf{F}(\boldsymbol{x}_i)) - \mathbf{S}_\mathrm{a}^{-1} (\boldsymbol{x}_i - \boldsymbol{x}_\mathrm{a}) \right], \quad (14)$$

where $\boldsymbol{x}_i$ is the vector state at the ith iteration, γ is the regularisation factor and $\mathbf{D}_i$ is the diagonal matrix (Gavin, 2015):

$$\mathbf{D}_i = \mathrm{diag} \left(\mathbf{K}_i^T \mathbf{S}_\epsilon^{-1} \mathbf{K}_i \right). \quad (15)$$

The matrix $\mathbf{K}_i$ is the Jacobian at the ith iteration given by

$$K_{ijl} = \frac{\partial F_j(\boldsymbol{x}_i)}{\partial x_l}. \quad (16)$$

In the case of an increasing χ^2, the values of the $\mathbf{K}_i$ matrix is determined by means of a finite difference calculation for $i = 0$ and every $2n$ iterations (with n number of parameters), while in the case of a decreasing χ^2, by using the Broyden rank-1 update formula (Broyden, 1965) for the quasi-Newton method:

$$\mathbf{K}_{i+1} = \mathbf{K}_i + \frac{\left[(\mathbf{F}(\boldsymbol{x}_{i+1}) - \mathbf{F}(\boldsymbol{x}_i) - \mathbf{K}_i \Delta \boldsymbol{x}_i) \Delta \boldsymbol{x}_i \right]}{\left(\Delta \boldsymbol{x}_i^T \cdot \Delta \boldsymbol{x}_i \right)}, \quad (17)$$

with $\Delta \boldsymbol{x}_i = \boldsymbol{x}_{i+1} - \boldsymbol{x}_i$.

The VCM of the state vector $\boldsymbol{x}$ is provided by the optimal estimation as follows (Rodgers, 2000):

$$\mathbf{S}_x = \left(\mathbf{K}^T \mathbf{S}_\epsilon^{-1} \mathbf{K} + \mathbf{S}_\mathrm{a}^{-1} \right)^{-1}. \quad (18)$$

The upwelling and downwelling radiances incoming at the cloud bottom and top respectively are simulated at each iteration. The obtained values are used for the calculation of the λ, D_- and D_+ coefficients in Eq. (1). For the simulation of the upwelling radiance, the emissivity of the surface is set to be equal to 1 and the ground temperature is equal to the value measured by a Vaisala VXT520 weather station placed on the roof of the same shelter where REFIR-PAD is installed.

4 Climatology and optimisation of the retrieved state vector

A study of the climatology of water vapour and temperature profiles has been performed using the entire radiosoundings dataset available for the year 2014 to calculate seasonal averages, shown in Fig. 3, and standard errors. In the right panel of Fig. 3 we can note the strong temperature inversion, a peculiar characteristic of the Antarctic atmosphere that occurs at about 500 m above ground during winter and autumn. Under these conditions the ground mean temperature can reach values below −60 °C. The water vapour VMR profiles also manifests a strong inversion in winter and autumn as shown in the left panel.

The standard deviation σ of the climatological profiles is used to calculate the a priori VCM. The range of the retrieved values is limited to $\pm 3\sigma$ in order to take into account the profile variability. Only for the ground level are larger ranges used, between 200 and 300 K for the temperature and between 1 and 3000 ppmv for the VMR. This choice allows us to take into account the much larger variability of the first layer that corresponds to the path inside the physics shelter. These ranges represent the real physical domain in which the atmospheric variables can be varied by the retrieval routine.

In order to determine how many degrees of freedom represent the atmospheric states and to choose the retrieval levels, a study of the matrix $\widetilde{\mathbf{K}}$ is defined as follows:

$$\widetilde{\mathbf{K}} = \mathbf{S}_y^{-\frac{1}{2}} \mathbf{K} \mathbf{S}_a^{\frac{1}{2}}, \tag{19}$$

which has been performed by means of the singular value decomposition (SVD):

$$\widetilde{\mathbf{K}} = Q \boldsymbol{\Sigma} \mathbf{V}^T. \tag{20}$$

Four seasonal climatological profiles, shown in Fig. 3, have been used to calculate the Jacobian with a vertical resolution of 100 m in clear sky conditions. $\boldsymbol{\Sigma}$ is a diagonal matrix of the singular values λ_i and $\mathbf{V}$ is a matrix with the columns $\widetilde{\boldsymbol{v}}_i$ that represent the eigenvectors of $\widetilde{\mathbf{K}}\widetilde{\mathbf{K}}^T$ in the state space transformed by $\mathbf{S}_a^{-\frac{1}{2}}$. To come back to the vector $\boldsymbol{v}_i$ in the original state space, we transform $\widetilde{\boldsymbol{v}}_i$ by means of $\mathbf{S}_a^{\frac{1}{2}}$ (Rodgers, 2000) according to

$$\boldsymbol{v}_i = \mathbf{S}_a^{\frac{1}{2}} \widetilde{\boldsymbol{v}}_i + \boldsymbol{x}_a. \tag{21}$$

As shown by Rodgers (2000), the singular values of $\widetilde{\mathbf{K}}$ represent the signal to noise ratio and the number of singular values, which are about or greater than one, represents the effective rank of the system. The singular values greater than one correspond to the states that carry information about the parameters to be retrieved; the lower ones don't bring information but only noise. The analysis shows that our measurement has about three degrees for water vapour and six for

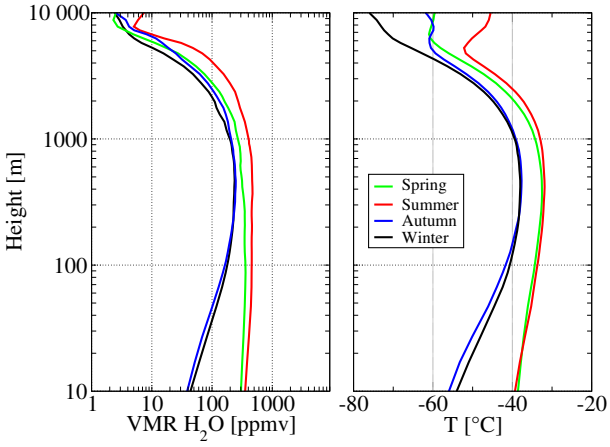

Figure 3. The four seasonal climatological profiles of water vapour VMR (left panel) and temperature (right panel) used as initial guesses in the fitting procedure.

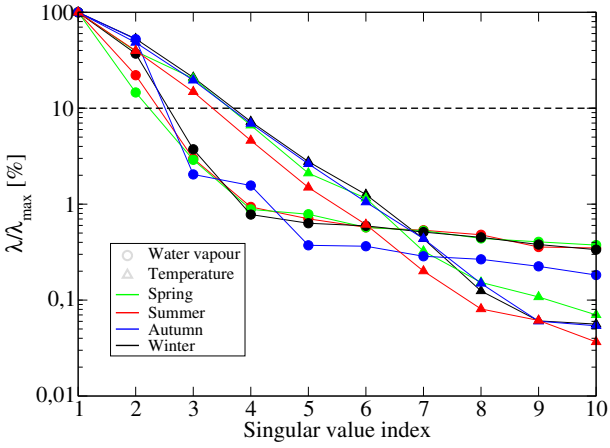

Figure 4. Trend of the ratios between the singular values λ_i and its maximum for water vapour (circles) and the temperature (triangles). The threshold used to select the singular independent states is represented by the black line.

temperature. The singular values also provide the sensitivity to measure a singular vector (Rodgers, 2000). To avoid the oscillation in the retrieval due to the strong variability in the lowest layers, only the singular vectors, which can be measured with a sensitivity greater than about 10 % of the maximum value have been taken into account in our analysis. These correspond to the first two eigenvectors for water vapour and the first three for temperature for all the seasons as shown in Fig. 4. Figure 5 shows, for example, the first three back-transformed singular vectors of $\widetilde{\mathbf{K}}$ for water vapour and temperature obtained by using the winter climatology.

The retrieval has been set up by choosing the first retrieved level at the ground in order to correctly take into account the effect of the very first atmospheric layers that are affected

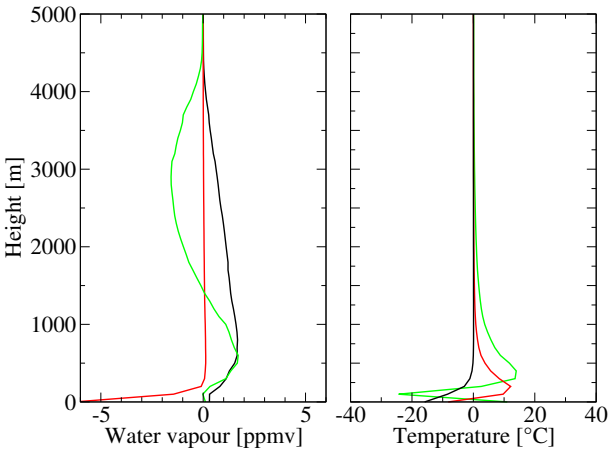

Figure 5. Back-transformed singular vectors of $\widetilde{\mathbf{K}}$ of water vapour and temperature for the first three singular values calculated by using the winter climatology.

by the presence of the shelter and the instrument itself. For the temperature, two other fitted levels are at about 10 and 300 m, whereas for water vapour, only one level at 200 m has been considered, which is sufficient to correctly rescale the humidity profile in the atmosphere above the first layer. The grid levels are then interpolated (linearly for temperature and logarithmically for water vapour) between the fitted levels, while the portion of the profile above the upmost fitted level is scaled according to the upmost value.

5 Data selection and results

The measurements of the downwelling spectral radiance used in this work were performed from the Antarctic station of Concordia using the REFIR-PAD spectroradiometer (Palchetti et al., 2015), which covers the 100–1400 cm^{-1} spectral range with a 0.4 cm^{-1} resolution. Each spectrum is on average 5 min of atmospheric observations. The measurement is repeated every 12 min due to the instrument calibration cycle. The instrument operates with a duty cycle of about 5 h out of 6.5 to allow for preanalysis and data transfer to Italy.

To evaluate the performances of the retrieval algorithm, we have selected exclusively measurements performed in presence of ice clouds and in a coincidence as close as possible with the radiosoundings routinely performed from Concordia at 12:00 UTC using Vaisala RS92 radiosondes. The cloud phase has been identified by analysing the logarithmic range-corrected signal (RCS) and the depolarisation component provided by the lidar every 10 min. We have identified 15 cases in which the above-mentioned requirements were all fulfilled in 2014. For each of these cases, we have selected the three spectra that were in better temporal coincidence with the 12:00 UTC radiosounding.

In Fig. 6 colour maps of the RCS and depolarisation signals detected by the lidar in coincidence with four of the selected REFIR-PAD measurements, one for each season, are shown. The red solid lines in the panels indicate the time of the REFIR-PAD acquisitions. Panel (a) shows the passage on 12 February 2014 of an ice cloud at 1.8 km of height with a geometrical thickness of about 1.4 km. The ice cloud in panel (b) occurred on 2 April 2014 at about 0.6 km of height with 1.4 km of thickness. Panel (c) shows the passage of an ice cloud on 10 August 2014 at 1 km with 2 km of thickness. Finally panel (d) shows a cloud at 1.6 km with 0.7 km of thickness on 1 October 2014. The vertical profiles of the RCS and depolarisation signals, shown in Fig. 7 for the measurements nearest to 12:00 UTC, allow us to infer the presence of a single ice phase and to exclude the cases of mixed-phase clouds that often occur in polar atmospheres (Turner, 2005; Turner et al., 2003; Pithan et al., 2014; Scott and Lubin, 2015).

Figure 8 shows the fitting results for the four selected cases of Fig. 6, taking only the measurements closer to the 12:00 UTC radiosounding. The measurements (black line) are compared with the synthetic spectra (red line) obtained by the fit. The fitting residuals are shown as a green line in the bottom of the plots. Panel (a) shows the atmospheric spectrum with an ice cloud composed of large-sized particles, the retrieval provided 47 µm of D_{ge} with an optical depth of 0.4. Panels (b) to (d) correspond to ice clouds with smaller diameters respectively 34, 21 and 23 µm and optical depths of 0.5, 1.1 and 0.6.

The comparison between the retrieved water vapour and temperature profiles with the radiosounding, in the four selected cases of Fig. 6, are presented in Fig. 9. As we can see the retrieved profiles generally agree with the radiosoundings measurements. Due to the low vertical resolution of the retrieval procedure, as also shown by the SVD analysis, it is not possible to capture the fine vertical structures visible in the radiosounding, e.g. the sharp variations occurring around 1000 m on 1 October 2014. Moreover, the lowermost fitted temperature point is not shown in the figure for the temperature due to several biases affecting its value:

1. the strong atmospheric variability occurring in the boundary layer,
2. the fact that the radiosonde is launched at about 500 m from the shelter where REFIR-PAD is located,
3. the presence of a very strong gradient in the first 3 m of the measurement path that includes the transition between the shelter and the external environment.

On the other side, above 5000 m, near the tropopause level, the downwelling spectral radiance has a negligible sensitivity to atmospheric water vapour and temperature, as shown by the SVD analysis (see Fig. 5).

In order to have an indication of the quality of the results for all the analysed cases, in Fig. 10 the retrieved pre-

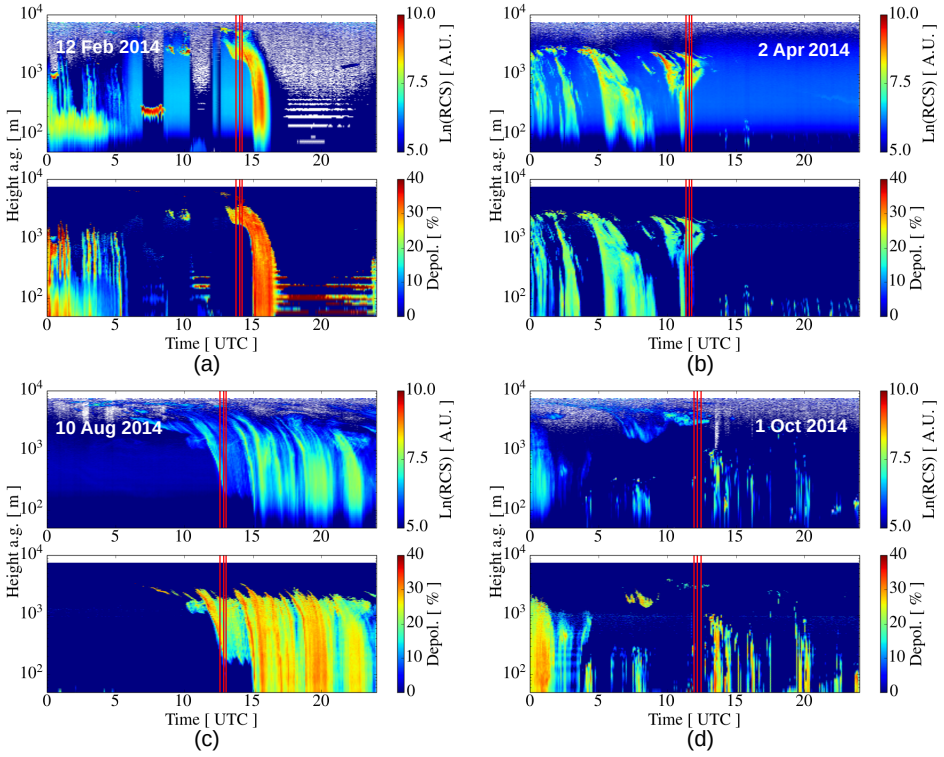

Figure 6. Colour maps of RCS and depolarisation signals performed by the lidar at Dome C for 4 selected days. The panels show the passage of an ice cloud in summer on 12 February 2014 **(a)**, in autumn on 2 April 2014 **(b)**, in winter on 10 August 2014 **(c)** and in spring on 1 October 2014 **(d)**. The red lines indicate the times at which the analysed spectra were acquired.

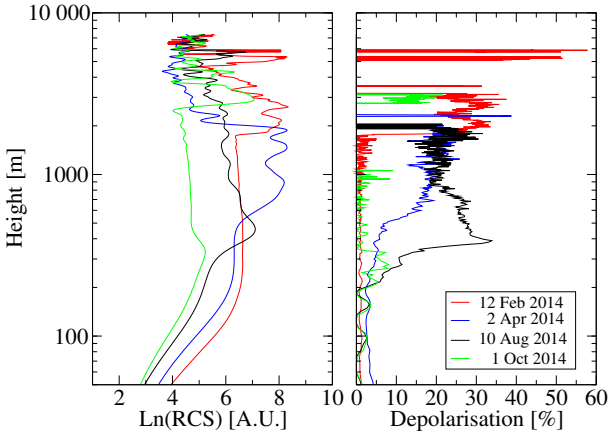

Figure 7. Logarithmic RCS and depolarisation signal corresponding to the 4 selected days in coincidence with the measurements nearest to 12:00 UTC.

cipitable water vapour (PWV) and the temperature of the inversion layer are compared with the corresponding values given by the radiosonde profiles in the top and middle panels respectively. The temperature of the inversion layer $T_{13\,\mathrm{m}}$, corresponding to the fitted level at 13 m above ground, is compared with the average temperature of the first 50 m above ground obtained by the radiosondes in order to take into account that the forward model used in the fitting process has a finite vertical resolution. The bottom panel shows the time difference between the retrieved measurements and the closed radiosonde profile. Figure 10 shows a generally good agreement between the retrieved and the radiosounding values, with the largest differences occurring when the measurements are in a less strict coincidence with the radiosonde launch and there is significant atmospheric variability, as in January, when the delay between REFIR-PAD measurements and radiosounding is about 2 h and the atmospheric state varies significantly (the three corresponding results are very different). Another condition in which we can expect greater differences is in wintertime, when the strong thermal inversion near ground affects the retrieval performance.

The fitting results for the cirrus cloud optical and microphysical properties are plotted as a function of time in Fig. 11 together with the cloud geometrical parameters inferred from the lidar measurements. The retrieved effective particle diameters D_e vary between 10 and 100 µm with an error lower than 20 %. The higher uncertainties occur for lower clouds with a thickness of about 300–500 m. The optical depths τ, calculated from the retrieved IWP by means of Eq. (3), are between 0.05 and 1.5. The errors, obtained through propagation from the retrieval error of the IWP, are less than 20 %.

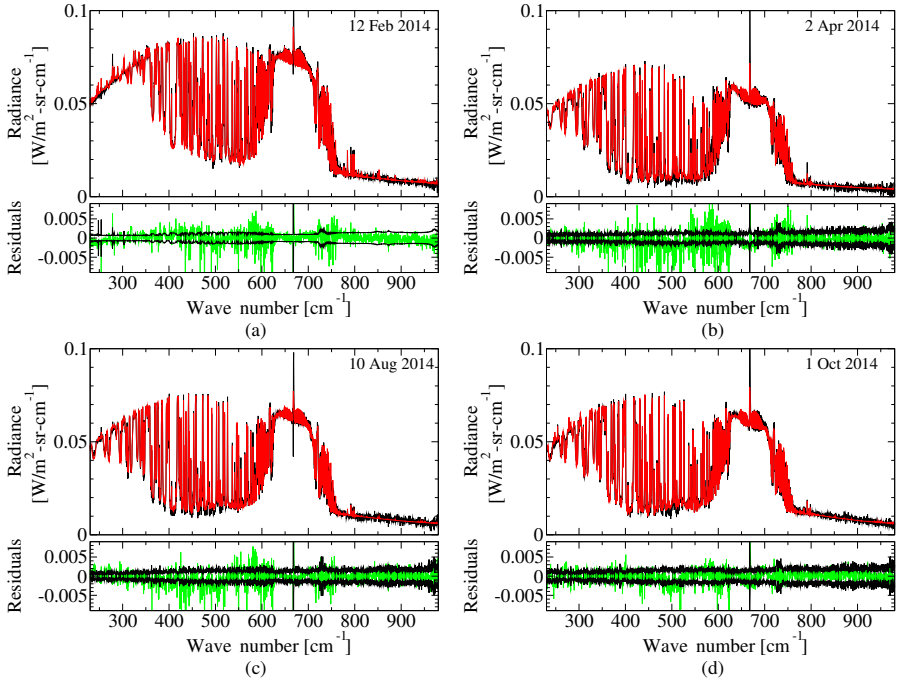

Figure 8. Comparisons of the synthetic spectra (red) provided by the retrieval with the measurements (black) nearest to 12:00 UTC for the same days shown in Fig. 6. The lower panels show the comparisons of the residuals (green) with the measurement uncertainty (black).

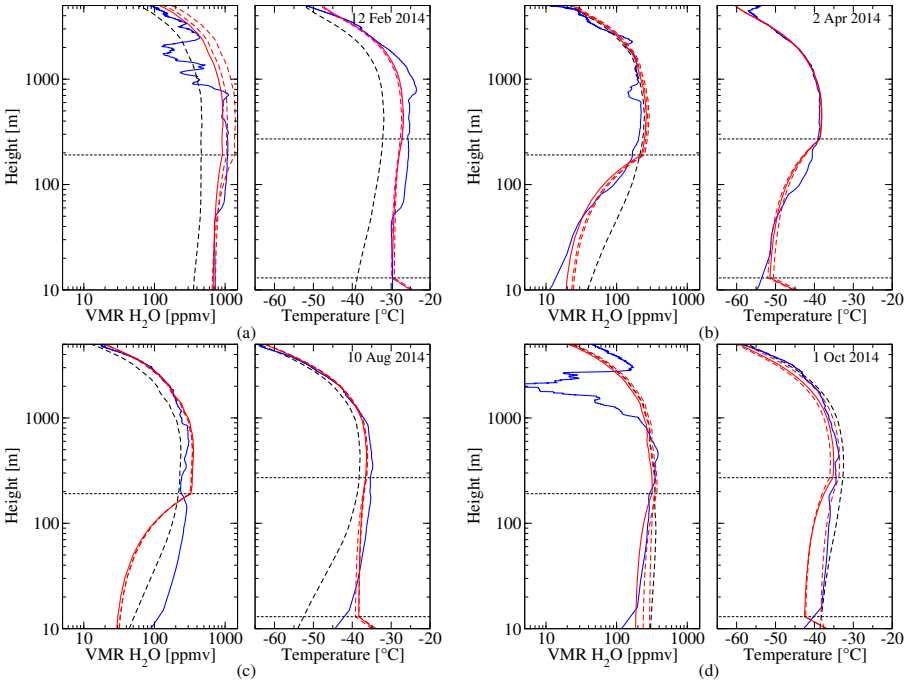

Figure 9. Comparison of the retrieved profiles of the water vapour VMR and temperature (red continuous and dashed line) for the selected measurements of Fig. 8 with the 12:00 UTC radiosounding profiles (blue) and the initial guess (dashed black line). The red continuous lines are related to the profile with better temporal coincidence with the radiosounding.

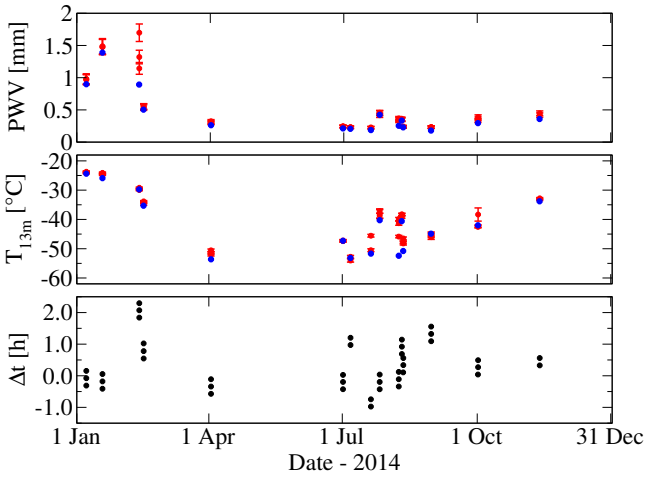

Figure 10. Comparison between the retrieved PWV and temperature of the inversion layer at 13 m above ground (red) with the corresponding radiosonde values (blue). For each radiosonde value, the figure shows the comparison with the retrieval of the two/three nearest spectra. The bottom panel shows the time difference between the spectrum acquisition and the corresponding radiosonde launch.

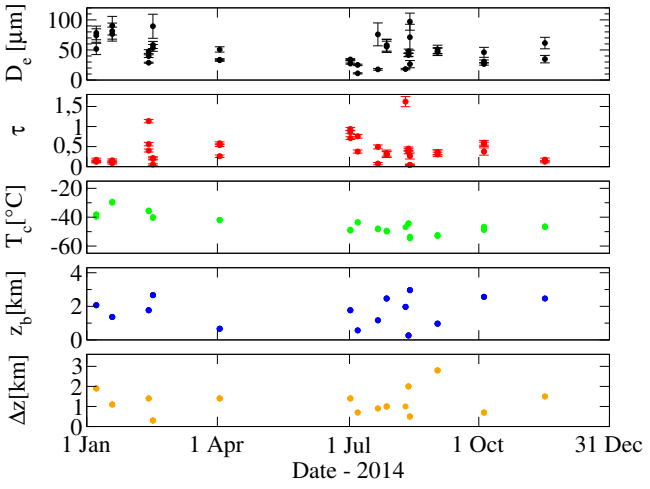

Figure 11. Time evolution of the retrieved cloud parameters: the generalised effective diameter D_e, optical depth τ, the cloud temperature T_c. The cloud bottom height z_b and the thickness Δz provided by the lidar are also shown.

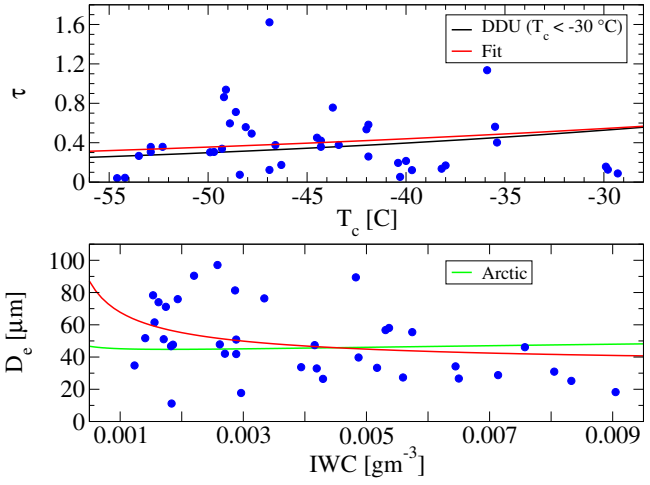

Figure 12. Retrieved data (blue) and fit (red) of optical depth as a function of temperature compared with the Dumont D'Urville (DDU) statistics (black) in the upper panel and with the Arctic D_e – IWC distribution (Liou et al., 2008) (green) in the lower panel.

The cloud temperature T_c, corresponding to the mean temperature between cloud top and bottom, is between −30 and −60 °C. T_c is obtained from the retrieved atmospheric profile using the cloud bottom height z_b and the thickness Δz provided by the lidar. We can see that the largest particle diameters occur in summer when temperatures are higher, as expected from the ice particle formation process, and the optical depths are generally lower than 1; hence the analysed cirrus clouds are optically thin (Mahesh et al., 2001b; Kahn et al., 2014). The retrieved cloud temperature is in most cases lower than −40 °C, which is consistent with the single phase of particles as detected by the lidar.

In order to have a first qualitative evaluation of the retrieval performance for the cloud parameters, we have also compared the retrieved distributions with the corresponding statistical distributions measured on the Antarctic coast at sea level at the Dumont d'Urville Station and in the Arctic. Specifically, the retrieved cloud parameters have been compared with two statistical correlations where τ is related to T_c and D_e to the ice water content (IWC). The first relationship is represented by an exponential function obtained from the data acquired at Dumont d'Urville in 1993 (Del Guasta et al., 1993) for cirrus clouds with a temperature lower than −30 °C and is given by

$$\tau = \exp(a \cdot T_c + b), \tag{22}$$

where $a = 0.0284$ and $b = 0.2110$.

The second relation correlates the effective diameter D_e with the IWC through a logarithmic relation given by (Liou et al., 2008):

$$D_e = \exp\left(a + b \cdot \ln(\mathrm{IWC}) + c \cdot (\ln(\mathrm{IWC}))^2\right), \tag{23}$$

where $a = 4.8510$, $b = 0.33159$ and $c = 0.026189$ are the coefficients obtained for the Arctic region. In our case, the values of IWC are calculated from the retrieved IWP, reflecting the assumption of a single uniform layer, as follows:

$$\mathrm{IWC} = \frac{\mathrm{IWP}}{\Delta z}, \tag{24}$$

where Δz is the geometrical thickness of the cloud.

The relationships of Eqs. (22) and (23) were used to fit the retrieved data varying the a, b and c coefficients, obtaining $a = 0.0212$ and $b = 0.0267$ for the $T_c - \tau$ case, and $a = 4.129$, $b = 0.3046$, and $c = 0.04591$ for the IWC $- D_e$ case.

The results of Fig. 12 show that the retrieval accuracy allows us to infer distribution laws for the retrieved cloud parameters that are compatible with analogous statistical distributions. A multi-year analysis over the full dataset of our measurements is under study in order to better quantify these distribution laws.

6 Conclusions

In this work an efficient code has been developed to perform the simultaneous retrieval of the atmospheric water vapour and temperature profiles and the cloud parameters, such as the generalised effective diameters and the ice water path. The code has been applied to the analysis of the measurements performed over the Antarctic Plateau in 2014 by the REFIR-PAD Fourier transform spectroradiometer. Acquired spectra have been analysed in the 230–980 cm^{-1} spectral range. In particular, the region below 667 cm^{-1} appears to be very important to characterise the ice particle size because in this region the spectrum modulation is strongly dependent on the particle size.

The modelling of the atmosphere has been performed by integrating the LBLRTM atmospheric forward model with a specifically developed code based on the δ-Eddington two-stream approximation of the radiative transfer to take into account the effect of clouds. A preliminary optimisation of the retrieved state vector has been performed by means of the Jacobian matrix to set the best retrieval grid for the water vapour and temperature profiles. A climatology study has also been performed by using daily radiosoundings available at Concordia station to provide good a priori information on the atmospheric variable correlation. Cloud position and phase detection are provided by the backscattering/depolarisation lidar installed near the REFIR-PAD instrument.

The fitting procedure allows to obtain a good agreement between measurements and simulations, with the residual differences generally falling within measurement noise over the whole relevant spectral range, including the FIR. The agreement is very good in the atmospheric window, where the radiative contribution depends exclusively on the optical and microphysical properties of the cloud and its temperature, whereas some differences occur in the FIR band because of the strong absorption due to water vapour and the extreme variability of its concentration. These conditions prevent achieving a high vertical resolution in the retrieval.

The retrieved atmospheric state and cloud parameters are also in generally good agreement with the supporting data available for the atmosphere. In particular, the atmospheric profiles of water vapour and temperature follow the available simultaneous radiosoundings, whereas the retrieved cirrus cloud parameters follow analogous statistical distributions available for polar regions.

This work has shown the capability to perform a simultaneous retrieval of the atmospheric state and cloud parameters from spectral measurements of the DLR over the Antarctic Plateau. By taking into account the whole spectral range in which the cloud infrared emission is relevant, it is able to disentangle the spectral interference between the variables. This process results in a better characterisation of the ice cloud radiative properties and will enable us to improve our understanding of their role in the Earth radiation budget.

7 Data availability

The dataset archive containing the emission spectra, the weather parameters, and the radiosoundings is being made publicly available at the REFIR website http://refir.fi.ino.it. Near-real-time acquisitions are shown every day online at http://refir.fi.ino.it/rtDomeC

The Supplement related to this article is available online at doi:10.5194/amt-10-825-2017-supplement.

Competing interests. The authors declare that they have no conflict of interest.

Acknowledgements. The deployment of REFIR-PAD in Antarctica was supported by the Italian National Program for Research in Antarctica PNRA (Programma Nazionale di Ricerche in Antartide) under the following projects: 2009/A04.03, 2013/AC3.01 and 2013/AC3.06. The authors are grateful to the research group of the Institute of Applied Physics Nello Carrara (CNR-Florence) composed by Bruno Carli, Simone Ceccherini, Marco Gai, Samuele Del Bianco, Ugo Cortesi, Marco Ridolfi, Piera Raspollini, Flavio Barbara, and Luca Sgheri of the Institute for the Applications of Calculus (CNR-Florence). for the precious and fruitful discussions.

Edited by: I. Moradi
Reviewed by: three anonymous referees

References

Baran, A. J.: The impact of cirrus microphysical and macrophysical properties on upwelling far infrared spectra, Q. J. Roy. Meteor. Soc., 133, 1425–1437, 2007.

Baran, A. J.: A review of the light scattering properties of cirrus, J. Quant. Spectrosc. Ra., 110, 1239–1260, 2009.

Baran, A. J.: The dependence of cirrus infrared radiative properties on ice crystal geometry and shape of the size-distribution function, Q. J. Roy. Meteor. Soc., 131, 1129–1142, 2015.

Baran, A. J., Hill, P., Furtado K., Field, P., and Manners, J.: A coupled cloud physics–radiation parameterization of the bulk optical properties of cirrus and its impact on the Met Office Uni-

fied Model Global Atmosphere 5.0 configuration, J. Climate, 27, 7725–7752, 2014.

Barton, N. P., Klein, S. A., and Boyle, J. S.: On the Contribution of Longwave Radiation to Global Climate Model Biases in Arctic Lower Tropospheric Stability, J. Climate, 27, 7250–7269, doi:10.1175/JCLI-D-14-00126.1, 2014.

Baum, B. A., Heymsfield, A. J., Yang, P., and Bedka, S. T.: Bulk scattering properties for the remote sensing of ice clouds. Part I: Microphysical data and models, J. Appl. Meteorol., 44, 1885–1895, 2005a.

Baum, B. A., Yang, P., Heymsfield, A. J., Platnick, S., King, M. D., Hu, Y., and Bedka, S. T.: Bulk scattering properties for the remote sensing of ice clouds. Part II: Narrowband models, J. Appl. Meteorol., 44, 1896–1911, 2005b.

Bianchini, G. and Palchetti, L.: Technical Note: REFIR-PAD level 1 data analysis and performance characterization, Atmos. Chem. Phys., 8, 3817–3826, doi:10.5194/acp-8-3817-2008, 2008.

Bianchini, G., Palchetti, L., and Carli, B.: A wide-band nadir-sounding spectroradiometer for the characterization of the Earth's outgoing long-wave radiation, Proc. SPIE, 6361, 63610A-1-11, doi:10.1117/12.689260, 2006.

Bianchini, G., Carli, B., Cortesi, U., Del Bianco, S., Gai, M., and Palchetti, L.: Test of far-infrared atmospheric spectroscopy using wide-band balloon-borne mmeasurements of the upwelling radiance, J. Quant. Spectrosc. Ra., 109, 1030–1042, 2008.

Bromwich, D. H., Nicolas, J. P., Hines, K. M., Kay, J. E., Key, E. L., Lazzara, M. A., Lubin, D., McFarquhar, G. M., Gorodetskaya, I. V., Grosvenor, D. P., Lachlan-Cope, T., and Van Lipzig, N. P. M.: Tropospheric clouds in Antarctica, Rev. Geophys., 50, RG1004, doi:10.1029/2011RG000363, 2012.

Broyden, C. G.: A class of methods for solving nonlinear simultaneous equations, Math. Comput., 19, 577–593, 1965.

Ceccherini, S. and Ridolfi, M.: Technical Note: Variance-covariance matrix and averaging kernels for the Levenberg–Marquardt solution of the retrieval of atmospheric vertical profiles, Atmos. Chem. Phys., 10, 3131–3139, doi:10.5194/acp-10-3131-2010, 2010.

Choi, Y.-S., Ho, C.-H., Kim, S.-W., and Lindzen, R. S.: Observational diagnosis of cloud phase in the winter antarctic atmosphere for parameterizations in climate models, Adv. Atmos. Sci., 27, 1233–1245, doi:10.1007/s00376-010-9175-3, 2010.

Clough, S. A., Shephard, M. W., Mlawer, E. J., Delamere, J. S., Iacono, M. J., Cady-Pereira, K., Boukabara, S., and Brown, P. D.: Atmospheric radiative transfer modeling: a summary of the AER codes, Short Communication, J. Quant. Spectrosc. Ra., 91, 233–244, 2005.

Cox, C. J., Turner, D. D., Rowe, P. M., Shupe, M. D., and Walden, V. P.: Cloud microphysical properties retrieved from downwelling infrared radiance measurements made at Eureka, Nunavut, Canada (2006–09), J. Appl. Meteorol. Clim., 53, 772–791, 2014.

Cox, C. J., Walden, V. P., Rowe, P. M., and Shupe, M. D.: Humidity trends imply increased sensitivity to clouds in a warming Arctic, Nat. Commun., 6, 10117, doi:10.1038/ncomms10117, 2015.

Cox, C. V., Harries, J. E., Taylor, J. P., Green, P. D., Baran, A. J., Pickering, J. C., Last, A. E., and Murray, J. E.: Measurement and simulation of mid-and far-infrared spectra in the presence of cirrus, Q. J. Roy. Meteor. Soc., 136, 718–739, 2010.

Deeter, M. N. and Evans, K. F.: A hybrid Eddington-single scattering radiative transfer model for computing radiances from thermally emitting atmospheres, J. Quant. Spectrosc. Ra., 60, 635–648, 1998.

De Leon, R. R. and Haigh, D. J.,Infrared properties of cirrus clouds in climate models, Q. J. R. Meteorol. Soc. 133: 273–282, 2007.

Del Guasta, M., Morandi, M., and Stefanutti, L.: One year of cloud lidar data from Dumont D'Urville (Antarctica) 1. General overview of geometrical and optical properties, J. Geophys. Res., 98, 18575–18587, 1993.

Fu, Q.: Parameterization of radiative processes in vertically nonhomogeneous multiple scattering atmospheres. PhD dissertation, Utah Univ., Salt Lake City, USA, avalaible from University Microfilm, 305 N. Zeeb Rd, Ann Arbor, MI 48106, 1991.

Fu, Q.: An accurate parameterization of the solar radiative properties of cirrus clouds for climate models, J. Climate, 9, 2058–2082, 1996.

Fu, Q. and Liou, K. N.: Parameterization of the radiative properties of cirrus clouds, J. Atmos. Sci., 50, 2008–2025, 1993.

Fu, Q., Yang, P., Sun, W. B.: An accurate parameterization of the infrared radiative properties of cirrus clouds for climate models, Am. Meteorol. Soc., 11, 2223–2237,1998.

Gavin, H. P.: The Levenberg–Marquardt method for nonlinear least squares curve-fitting problems, Department of Civil and Environmental Engineering, Duke University, available at: http://people.duke.edu/~hpgavin/ce281/lm.pdf (last access: 28 February 2017), September 2015.

Hardiman, S. C., Boutle, I. A., Bushell, A. C., Butchart, N., Cullen, M. J. P., Field, P. R., Furtado, K., Manners, J. C., Milton, S. F., Morcrette, C., O'Connor, F. M., Shipway, B. J., Smith, C., Walters, D. N., Willett, M. R., Williams, K. D., Wood, N., Abraham, N. L., Keeble, J., Maycock, A. C., Thuburn, J., and Woodhouse, M. T.: Processes Controlling Tropical Tropopause Temperature and Stratospheric Water Vapor in Climate Models, J. Climate, 28, 6516–6535, doi:10.1175/JCLI-D-15-0075.1, 2015.

Harries, J., Carli, B., Rizzi, R., Serio, C., Mlynczak, M., Palchetti, L., Maestri, T., Brindley, H., and Masiello, G.: The Far Infrared Earth, Rev. Geophys., 46, RG4004, doi:10.1029/2007RG000233, 2008.

Huang, Y., Leroy, S., Gero, P. J., Dykema, J., and Anderson, J.: Separation of longwave climate feedbacks from spectral observations, J. Geophys. Res., 115, D07104, doi:10.1029/2009JD012766, 2010.

Joseph, J. H. and Wiscombe, W. J.: The delta-Eddington approximation for radiative flux transfer, J. Atmos. Sci., 33, 2452–2459, 1976.

Kahn, B. H., Irion, F. W., Dang, V. T., Manning, E. M., Nasiri, S. L., Naud, C. M., Blaisdell, J. M., Schreier, M. M., Yue, Q., Bowman, K. W., Fetzer, E. J., Hulley, G. C., Liou, K. N., Lubin, D., Ou, S. C., Susskind, J., Takano, Y., Tian, B., and Worden, J. R.: The Atmospheric Infrared Sounder version 6 cloud products, Atmos. Chem. Phys., 14, 399–426, doi:10.5194/acp-14-399-2014, 2014.

Kiehl, J. T. and Trenberth, K. E.: Earth's annual global mean energy budget, B. Am. Meteorol. Soc., 78, 197–207, 1997.

Liou, K.: Influence of cirrus clouds on weather and climate processes:a global perspective, Mon. Weather Rev., 114, 1167–1199, 1986.

Liou, K. N., Gu, Y., Yue, Q., and McFarguhar, G.: On the correlation between ice water content and ice crystal size and its appli-

cation to radiative transfer and general circulation models, Geophys. Res. Lett., 35, L13805, doi:10.1029/2008GL033918, 2008.

Lubin, D., Chen, B., Bromwich, D. H., Somerville, R. C. J., Lee, W. H., and Hines, K. M.: The impact of Antarctic cloud radiative properties on a GCM climate simulation, J. Climate, 11, 447–462, doi:10.1175/1520-0442(1998)011<0447:tioacr>2.0.co;2, 1998.

Lubin, D., Kahn, B. H., Lazzara, M. A., Rowe, P., and Walden, V. P.: Variability in AIRS-retrieved cloud amount and thermodynamic phase over west versus east Antarctica influenced by the SAM, Geophys. Res. Lett., 42, 1259–1267, 2015.

Lynch, D., Sassen, K., Star, D. O., and Stephens G. (Eds.): Cirrus, Oxford University Press, Inc., New York, 2002.

Maestri, T. and Holz, R. E.: Retrieval of cloud optical properties from multiple infrared hyperspectral measurements: A methodology based on a line-by-line multiple-scattering code, IEEE T. Geosci. Remote, 47, 2413–2426, 2009.

Maestri, T., Rizzi, R., and Smith, J. A.: Spectral infrared analysis of a cirrus cloud based on Airborne Research Interferometer Evaluation System (ARIES) measurements, J. Geophys. Res.-Atmos., 110, D06111, doi:10.1029/2004JD005098, 2005.

Maestri, T., Rizzi, R., Tosi, E., Veglio, P., Palchetti, L., Bianchini, G., Di Girolamo, P., Masiello, G., Serio, C., and Summa, D.: Analysis of cirrus cloud spectral signatures in the far infrared, J. Quant. Spectrosc. Ra., 141, 49–64, 2014.

Mahesh, A., Walden, V. P., and Warren, S. G.: Ground-Based Infrared Remote Sensing of Cloud Properties over the Antarctic Plateau. Part I: Cloud-Base Heights, J. Appl. Meteorol., 40, 1265–1278, doi:10.1175/1520-0450(2001)040<1265:GBIRSO>2.0.CO;2, 2001a.

Mahesh, A., Walden, V. P., and Warren, S. G.: Ground-Based Infrared Remote Sensing of Cloud Properties over the Antarctic Plateau. Part II: Cloud Optical Depths and Particle Sizes, J. Appl. Meteorol., 40, 1279–1294, doi:10.1175/1520-0450(2001)040<1279:GBIRSO>2.0.CO;2, 2001b.

Mahesh, A., Campbell, J. R., and Spinhirne, J. D.: Multi-year measurements of cloud base heights at South Pole by lidar, Geophys. Res. Lett., 32, L09812, doi:10.1029/2004GL021983, 2005.

Marquardt, D. W.: An algorithm for least-squares estimation of nonlinear parameters, SIAM J. Appl. Math., 11, 431–441, 1963.

Palchetti, L., Bianchini, G., Castagnoli, F., Carli, B., Serio, C., Esposito, F., Cuomo, V., Rizzi, R., and Maestri, T.: Breadboard of the Fourier transform spectrometer for the Radiation Explorer in the Far Infrared (REFIR) atmospheric mission, Appl. Optics, 44, 2870–2878, 2005.

Palchetti, L., Bianchini, G., Carli, B., Cortesi, U., and Del Bianco, S.: Measurement of the water vapour vertical profile and of the Earth's outgoing far infrared flux, Atmos. Chem. Phys., 8, 2885–2894, doi:10.5194/acp-8-2885-2008, 2008.

Palchetti, L., Bianchini, G., Di Natale, G., and Del Guasta, M.: Far-Infrared radiative properties of water vapor and clouds in Antarctica, B. Am. Meteorol. Soc., 96, 1505–1518, doi:10.1175/BAMS-D-13-00286.1, 2015.

Palchetti, L., Di Natale, G., and Bianchini, G.: Remote sensing of cirrus microphysical properties using spectral measurements over the full range of their thermal emission, J. Geophys. Res., 121, 10804–10819, doi:10.1002/2016JD025162, 2016.

Pithan, F., Medeiros, B., and Mauritsen T.: Mixed-phase clouds cause climate model biases in Arctic wintertime temperature inversions, Clim. Dynam., 43, 289, 289–303, doi:10.1007/s00382-013-1964-9, 2014.

Rathke, C. and Fisher, J.: Retrieval of cloud microphysical properties from thermal infrared observations by a fast iterative radiance fitting method, J. Atmos. Ocean. Tech., 17, 1509–1524, 2000.

Remedios, J. J., Leigh, R. J., Waterfall, A. M., Moore, D. P., Sembhi, H., Parkes, I., Greenhough, J., Chipperfield, M. P., and Hauglustaine, D.: MIPAS reference atmospheres and comparisons to V4.61/V4.62 MIPAS level 2 geophysical data sets, Atmos. Chem. Phys. Discuss., 7, 9973–10017, doi:10.5194/acpd-7-9973-2007, 2007.

Rodgers, C. D.: Inverse Methods for Atmospheric Sounding: Theory and Practice, World Scientific Pub Co Inc., Singapore, 2000.

Sassen, K., Wang, Z., and Liu, D.: Global distribution of cirrus clouds from CloudSat/Cloud-Aerosol lidar and infrared pathfinder satellite observations (CALIPSO) measurements, J. Geophys. Res.-Atmos., 113, D00A12, doi:10.1029/2008JD009972, 2008.

Scott, R. C. and Lubin, D.: Unique manifestations of mixed-phase cloud microphysics over Ross Island and the Ross Ice Shelf, Antarctica, Geophys. Res. Lett., 43, 2936–2945, doi:10.1002/2015GL067246, 2015.

Stocker, T. F., Quin, D., Plattner, G.-K., Tignor, M. M. B., Allen, S. K., Boschun, J., Nauels, A., Xia, Y., Bex, V., and Midgley, P. M.: IPCC, 2013: climate change 2013: the physical science basis. Contribution of working group I to the fifth assessment report of the intergovernmental panel on climate change, Cambridge University Press, Switzerland, 2013.

Turner, D. D.: Arctic Mixed-Phase Cloud Properties from AERI Lidar Observations: Algorithm and Results from SHEBA, J. Appl. Meteorol., 44, 427–444, 2005.

Turner, D. D., Ackerman, S. A., Baum, B. A., Revercomb, H. E., and Yang, P.: Cloud Phase Determination Using Ground-Based AERI Observations at SHEBA, J. Appl. Meteorol., 42, 710–715, 2003.

Wiser, K. and Yang, P.: Average ice crystal size and bulk shortwave single-scattering properties of cirrus clouds, Atmos. Res., 49, 315–335, 1998.

Wylie, D. P. and Menzel, W. P.: Eight Years of High Cloud Statistics Using HIRS, J. Climate, 12, 170–184, 1999.

Yang, P., Gao, B. C., Baum, B. A., Hu, Y. X., Wiscombe, W. J., Tsay, S. C., Winker, D. M., and Nasiri, S. L.: Radiative properties of cirrus clouds in the infrared (8– 13 mm) spectral region, J. Quant. Spectrosc. Ra., 70, 473–504, 2001.

Yang, P., Wei, H., Huang, H.-L., Baum, B. A., Hu, Y. X., Kattawar, G. W., Mishchenko, M. I., and Fu, Q.: Scattering and absorption property database for nonspherical ice particles in the near-through far-infrared spectral region, Appl. Optics, 44, 5512–5522, 2005.